

Interaction of cellular and network mechanisms for efficient pheromone coding in moths

Hana Belmabrouk^a, Thomas Nowotny^b, Jean-Pierre Rospars^c, and Dominique Martinez^{a,1}

^aLaboratoire Lorrain de Recherche en Informatique et ses Applications (LORIA) Unité Mixte de Recherche 7503, Centre National de la Recherche Scientifique, 54506 Vandœuvre-lès-Nancy, France; ^bCentre for Computational Neuroscience and Robotics (CCNR), University of Sussex, Falmer, Brighton BN1 9QJ, United Kingdom; and ^cUnité Mixte de Recherche 1272 Physiologie de l'Insecte Signalisation et Communication (PISC), Institut National de la Recherche Agronomique, 78026 Versailles, France

Edited by John G. Hildebrand, University of Arizona, Tucson, AZ, and approved October 27, 2011 (received for review July 29, 2011)

Sensory systems, both in the living and in machines, have to be optimized with respect to their environmental conditions. The pheromone subsystem of the olfactory system of moths is a particularly well-defined example in which rapid variations of odor content in turbulent plumes require fast, concentration-invariant neural representations. It is not clear how cellular and network mechanisms in the moth antennal lobe contribute to coding efficiency. Using computational modeling, we show that intrinsic potassium currents (I_A and I_{SK}) in projection neurons may combine with extrinsic inhibition from local interneurons to implement a dual latency code for both pheromone identity and intensity. The mean latency reflects stimulus intensity, whereas latency differences carry concentration-invariant information about stimulus identity. In accordance with physiological results, the projection neurons exhibit a multiphasic response of inhibition–excitation–inhibition. Together with synaptic inhibition, intrinsic currents I_A and I_{SK} account for the first and second inhibitory phases and contribute to a rapid encoding of pheromone information. The first inhibition plays the role of a reset to limit variability in the time to first spike. The second inhibition prevents responses of excessive duration to allow tracking of intermittent stimuli.

olfaction | pheromone plume | odor coding | concentration invariance | small conductance channel

To attract conspecific males, female moths release volatile blends of a few chemical compounds, so-called sex pheromones. Most pheromone compounds are hydrocarbon molecules emitted in the right proportions for biological relevance. Sympatric species often share the same chemicals but in different proportions [e.g., *Heliothis zea* and *H. virescens* (1, 2) or *Yponomeuta cagnagellus*, *Y. irrorellus*, and *Y. plumbellus* (3)]. To prevent cross-attraction, the pheromone blend is distinguishable not only by the identity of the individual components but also by their precise ratio. Behavioral experiments revealed that male moths are tuned to the specific proportions emitted by their conspecific females. Slight changes in component ratios, for example, can inhibit the anemotactic response of males of one species, while attracting males from another species (4–6). Pheromones are passively transported in the air and mixed by atmospheric turbulence, and therefore, during flight, male moths encounter pheromone filaments with all components present in the same proportions as released (7) but over a broad range of concentrations (8, 9). In the race for mating, flying male moths have to solve a difficult pattern recognition problem (i.e., recognize, in real time, pheromone compounds and their proportions independently of blend concentration). To do so, the information delivered by olfactory receptor neurons (ORNs) is integrated in the antennal lobe by a neural network involving inhibitory local neurons (LNs) and excitatory projection neurons (PNs). All synaptic connections between these neurons take place in a subset of enlarged, sexually dimorphic glomeruli, the macroglomerular complex (MGC). The circuitry of the MGC is similar to the one of the generalist olfactory subsystem. In the generalist subsystem, prolonged odor stimulations (up to several seconds) create local field potential oscillations and transient PN assemblies that synchronize to them

and evolve in time in a stimulus-specific manner (10–12). Using time in such a manner as a coding dimension, however, poses a serious problem for a flying insect. In natural plumes, odor contacts with the antennae are brief and intermittent, with up to five contacts per 1 s and each contact lasting down to under 20 ms (13, 14). Consequently, responses in the olfactory system have to be fast. In *Drosophila*, for example, upwind surges generally begin 85 ms after ORN onset (15). During this time frame, the PNs cannot fire many more than 10 spikes (assuming mean rates of 120 spikes/s and 0 ms latency). Recordings from moths in natural conditions revealed that MGC-PNs produce 3–28 spikes after each pheromone contact on the antennae, depending on stimulus intensity (figures 3 and 4 in ref. 13). These observations put strong time constraints on the optimization of pheromone representations for concentration-invariant recognition. Given the discontinuous nature of the odor cues, how does the MGC achieve stable representations in less than 100 ms? How is the pheromone encoded with only a few spikes per PN?

In this work, we address this fundamental question for the olfactory system of the moth *Manduca sexta*, which is one of the best-characterized olfactory systems. In natural conditions, male *M. sexta* moths are attracted by a blend of two main compounds of the sex pheromone in a proportion of 2:1 (16). The primary natural component is E,Z-10,12-hexadecadienal [bombykal (BAL)]. The second natural component, E,E,Z-10,12,14-hexadecatrienal, is often replaced by a more stable chemical E,Z-11,13-pentadecadienal (C15) in laboratory experiments (17). For simplicity, we will refer to both BAL and C15 as natural pheromone components. MGC-PNs are classified as specialists or generalists according to their responses to single compounds (18, 19). Generalist PNs are excited by BAL and C15, whereas specialist PNs are excited by one compound and inhibited by the other (19, 20). BAL or C15 specialist PNs fire synchronously, and their synchronization is sharpened by the presence of both components in the pheromone mixture (21). With the blend, they exhibit a multiphasic discharge pattern, either inhibition–excitation–inhibition ($I_1/E/I_2$) or excitation–inhibition (E/I_2) (18). The goal of our work was to highlight extrinsic and intrinsic neuronal mechanisms that would lead to the experimentally observed distribution of response properties and to investigate how pheromone blends are encoded or represented by such PN multiphasic discharge patterns. The origin of this multiphasic patterning is unclear. I_2 , for example, was abolished by certain GABA_A antagonists [e.g., bicuculline (BIC)] and not by others [e.g., picrotoxin (PTX)] (22). Differences in BIC and PTX sensitivity might be explained by the fact that a subunit of the GABA_A receptor is PTX-sensitive and BIC-insensitive (23). However, I_2 was relatively unaffected by changes in chloride

Author contributions: H.B. and D.M. designed research; H.B. performed research; T.N. and J.-P.R. contributed new reagents/analytic tools; H.B. and D.M. analyzed data; and D.M. wrote the paper.

The authors declare no conflict of interest.

This article is a PNAS Direct Submission.

¹To whom correspondence should be addressed. E-mail: Dominique.Martinez@loria.fr.

This article contains supporting information online at www.pnas.org/lookup/suppl/doi:10.1073/pnas.1112367108/-DCSupplemental.

concentrations, which makes the role of GABAergic synapses questionable (24). Interestingly, BIC has been shown to block a calcium-dependent potassium channel, the small conductance (SK) channel (25, 26), and Ca^{2+} -dependent K^+ currents as well as transient A-type K^+ currents have been identified in the PNs of *M. sexta* (27, 28). Questions previously raised find specific formulations here. Do intrinsic K^+ currents (A-type or Ca^{2+} -dependent K^+) combine with network mechanisms (inhibition from LNs) to shape the multiphasic response? How do inhibitory and excitatory phases contribute to efficient coding of pheromone? Do generalist and specialist PNs play different roles in this coding? In this work, we address these questions by means of computational modeling using a detailed MGC model of *M. sexta* moths.

Results

MGC Model Reproduces Physiological Firing Patterns. Experimental studies have revealed that the MGC of male *M. sexta* moths contains two types of inhibitory LNs (IIa and IIb) (29). Both LN types are multiglomerular but differ in their pattern of connectivity and their response to the pheromone. LNs-IIa have very dense branches in the MGC and exhibit brief and phasic excitatory responses (figure 17 in ref. 29). On the contrary, LNs-IIb possess a less dense arborization, and their response to the pheromone blend is a long-lasting tonic discharge (figure 19 in ref. 29). MGC-PNs are classified as specialist or generalist according to their responses to single compounds (18, 19). Generalist PNs are excited by both compounds C15 and BAL ($n = 13$; 32% of the PNs in table 1 in ref. 18). Specialist PNs are inhibited by one compound and excited by the other. They exhibit a complex discharge pattern with the blend of either excitation–inhibition (biphasic pattern E/I_2 in 39% of the PNs) or inhibition–excitation–inhibition (triphasic pattern $\text{I}_1/\text{E}/\text{I}_2$ in 29% of the PNs).

As described in *Methods*, we developed a detailed model of the *M. sexta* MGC that fits the numbers used in refs. 18 and 29 (i.e., 86 LNs-IIa, 68 LNs-IIb, and 41 PNs). A schema of the model is shown in Fig. S1. We investigated whether this model reproduces the different types of responses in the correct proportions. In line with the experimental data (figures 17 and 19 in ref. 29), LNs-IIa and LNs-IIb in our MGC model responded to blend-like stimuli, with short- and long-lasting firing patterns, respectively (Fig. 1A). Generalist and specialist responses of the PNs were also reproduced (Fig. 1B). Their proportions, however, depended on the probabilities of connection $p(\text{LN-IIa} \rightarrow \text{PN})$ from LNs-IIa to PNs and $p(\text{LN-IIb} \rightarrow \text{PN})$ from LNs-IIb to PNs. To quantify the plausibility of the model, we computed the Kullback–Leibler distance (KLD) between the proportions of PN responses obtained with the model and the real proportions observed in experimental data (gray-coded areas vs. areas delimited by red lines in the pie chart in Fig. 1B). The KLD equals zero when the model reproduces exactly the biological responses in the right proportions. For each pair of probabilities $p(\text{LN-IIa} \rightarrow \text{PN})$ and $p(\text{LN-IIb} \rightarrow \text{PN})$, 30 MGC networks were randomly generated and simulated during 1 s biological time. The PNs were classified automatically with an algorithm identifying their responses to the blend and single compounds. The KLD (mean and SD) was estimated over the different runs (*Methods* and *SI Text, Model*). As expected, the KLD depended on LN to PN connectivity (Fig. 1C). The existence of a minimum at $p(\text{LN-IIa} \rightarrow \text{PN}) = 0.5$ and $p(\text{LN-IIb} \rightarrow \text{PN}) = 0.2$ suggests that the PNs should be more densely connected to the LNs-IIa than the LNs-IIb to reproduce physiological firing patterns (Fig. 1D). This result is in line with experimental data revealing a dense and a sparse glomerular innervation for LNs-IIa and LNs-IIb, respectively (29). Although the minimal KLD is 1.33 and not 0, the PN responses and their proportions obtained in simulation are in good agreement with those obtained experimentally (Fig. 1B).

Roles of Extrinsic Properties: LNs-IIa and LNs-IIb. From the previous section, it becomes clear that inhibition from LNs plays a role in shaping the PN response. However, LNs-IIa and LNs-IIb have different firing responses and connectivity patterns (Fig. 1A and D). To separate the potentially different influences of LNs-IIa and

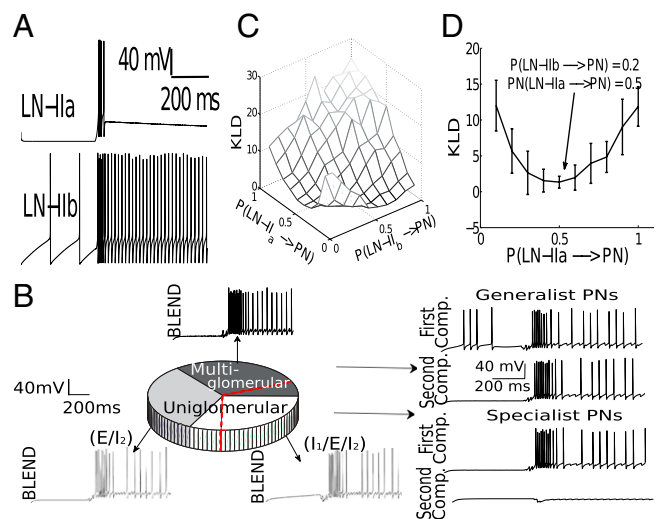


Fig. 1. Response patterns in the intact MGC network model. (A) Typical LN responses (86 LNs-IIa and 68 LNs-IIb). The LNs-IIa responded to pheromone-like stimuli with a short burst of spikes. On the opposite end, the LNs-IIb exhibited prolonged tonic responses. (B) Typical PN response patterns extracted from the MGC model (41 PNs). From their response to single compounds, the PNs were classified as specialist or generalist. Generalist PNs (30% of the PNs; dark area in pie chart) were excited by both compounds, C15 and BAL, whereas specialist PNs were inhibited by one compound and excited by the other. When we looked at the network connectivity, we noticed that generalist and specialist PNs were multiglomerular and uniglomerular, respectively. Specialist PNs responded to the blend with a complex temporal pattern, either biphasic with excitation–inhibition, denoted E/I_2 (37% of the PNs; gray area in pie chart), or triphasic with inhibition–excitation–inhibition, denoted $\text{I}_1/\text{E}/\text{I}_2$ (33% of the PN; white area in pie chart). The proportions of response patterns, 30%–37%–33% for the generalists and biphasic and triphasic specialists, were obtained on 30 MGC networks randomly generated with $p(\text{LN-IIa} \rightarrow \text{PN}) = 0.5$ and $p(\text{LN-IIb} \rightarrow \text{PN}) = 0.2$ and simulated during 1 s of biological time. The real proportions (areas delimited by red lines in the pie chart) observed in experimental data are 32%–39%–29% (29). The Kullback–Leibler distance (KLD) between the real proportions and those proportions obtained with the model was $\text{KLD} = 1.33$. (C) Capability for the MGC model to reproduce the physiological responses for different probabilities of connection $p(\text{LN-IIa} \rightarrow \text{PN})$ and $p(\text{LN-IIb} \rightarrow \text{PN})$. The KLD is zero when the model reproduces the physiological responses in the right proportions. The proportions of response patterns were obtained, for each pair of probabilities $p(\text{LN-IIa} \rightarrow \text{PN})$ and $p(\text{LN-IIb} \rightarrow \text{PN})$ on 30 random MGC networks (simulations of 1 s). (D) The MGC model is optimal for $p(\text{LN-IIa} \rightarrow \text{PN}) = 0.5$ and $p(\text{LN-IIb} \rightarrow \text{PN}) = 0.2$. At this point, $\text{KLD} = 1.33$, and the PN responses with their proportions are illustrated in B.

LNs-IIb, we selectively removed each type of LNs from the MGC network and analyzed the PN responses. Without LN-IIa, the triphasic patterns were lost (Fig. S24). The biphasic patterns represented 68% of the PNs, which corresponds to the proportions of biphasic plus triphasic patterns in the intact network. These results indicate that removing LNs-IIa from the network changed the patterns from triphasic ($\text{I}_1/\text{E}/\text{I}_2$) to biphasic (E/I_2). LNs-IIa are, therefore, responsible for I_1 in the triphasic patterns. As for I_2 , the analysis did not reveal any particular role for LNs-IIa. The same procedure was applied to study the role of the LNs-IIb. Removing the LNs-IIb did not disturb the proportions of the PNs responses (same pie chart as for the intact network in Fig. 1B). However, although I_2 did not disappear from the multiphasic responses, its duration was significantly reduced (106 ± 2.68 ms without LNs-IIb vs. 112 ± 5 ms for the intact network, $P < 0.05$, Kruskal–Wallis test) (Fig. S2B). We, therefore, concluded that the LNs-IIb are involved in but not solely responsible for I_2 .

Another putative role for the LNs is to synchronize the PNs. In the MGC of male *M. sexta*, BAL or C15 specialist PNs fire in synchrony when activated by pheromone stimulation to the antenna (21). Interestingly, greater synchrony is obtained with the blend

than single compounds. To assess whether our model can reproduce these data, we examined the precise timings of spikes and computed the level of synchrony as the percentage of synchronized spikes within 150 ms after stimulus onset (*Methods*). The data reported in Fig. S2C are means and SDs estimated over 30 trials. In the intact MGC model, BAL or C15 PNs are more synchronized with the blend ($69 \pm 27\%$) than with single compounds ($59 \pm 26\%$). Simulation data are in agreement with experiments (figure 4c in ref. 21). Is greater PN synchrony with the blend attributable to more vigorous inhibition from more strongly activated LNs? To answer this question, we selectively removed each type of LNs from the MGC network. The consequence was a decrease in synchrony from $69 \pm 27\%$ for the intact MGC model to $51 \pm 23\%$ for the model without LN-IIa and $56 \pm 28\%$ for the model without LN-IIb (Fig. S2C) ($P < 0.05$, Kruskal–Wallis test followed by Mann–Whitney test). Although both LN types are involved in PN synchrony, removing the LNs-IIa had significantly more impact. The LNs-IIa contribute more to PN synchrony, because the PNs are more densely connected to the LNs-IIa than to the LNs-IIb [$p(\text{LN-IIa} \rightarrow \text{PN}) = 0.5$ vs. $p(\text{LN-IIb} \rightarrow \text{PN}) = 0.2$]. To understand how LNs-IIa synchronize the PNs, we analyzed the PN activities in the intact MGC network and the same network with the LNs-IIa blocked. In the intact network, we observed that inhibition I_1 arose before the E response (representative voltage traces of two PNs are represented in Fig. S2D). During the I_1 phase, the PNs have a tendency to forget their initial conditions by relaxing their activity to a hyperpolarized quasi-steady state. As a consequence, the neurons fire synchronously when inhibition is removed. On the contrary, in the network where the LNs-IIa were blocked, the I_1 phase disappeared or was not strong enough to play the role of a reset and eliminate the influence of initial conditions (Fig. S2D).

Roles of Intrinsic Properties: I_A and I_{SK} . The above observations indicate that enhancement of PN synchrony is attributable to a loss of initial conditions and can be interpreted in terms of a reset by inhibition. A prerequisite to have synchronization in the first place is that inhibition from LNs arises before the PN response (I_1 before E), which implies that LNs need to fire before PNs. In agreement with this hypothesis, first spike latencies were significantly shorter for LNs than PNs (19 ± 3 ms for LN-IIa and 3 ± 1.5 ms for LN-IIb vs. 54 ± 18 ms for PNs, $P < 0.05$, Kruskal–Wallis test followed by Mann–Whitney test) (Fig. 2A). What intrinsic current

could explain the significant delay to the first spike in PNs compared with LNs? When the A current was blocked, PNs fired earlier (latency was 54 ± 18 ms for intact PNs and 26 ± 22 ms with I_A blocked, $P < 0.05$, Kruskal–Wallis test) (Fig. 2A). Thus, the firing delay in PNs resulted from the action of the A current. Fast activation of the transient K^+ current prevented the PNs from firing immediately in response to a depolarization. When the A current was blocked, the PNs were also less synchronized (synchrony level = $69 \pm 27\%$ for intact PNs and $66 \pm 23\%$ with I_A blocked, $P < 0.05$, Kruskal–Wallis test) (Fig. 2B). The decrease in synchrony when I_A is blocked is, therefore, attributable to earlier PN firings, which makes the reset by I_1 less effective.

Previous simulations highlighted the causes and effects of I_1 . As for I_2 , experimental data revealed that it is abolished by BIC and not PTX (22) and that a calcium-dependent potassium channel, the SK channel, is BIC-sensitive (25, 26). Given that I_2 remained relatively unchanged in the MGC model without LNs, as seen above, could it be produced by the SK current? Blocking I_{SK} did not disturb the proportions of the PN responses (same pie chart as for the intact network in Fig. 1B), but I_2 disappeared from the multiphasic responses (Fig. 2C). Triphasic ($I_1/E/I_2$) patterns were changed to biphasic (I_1/E), and biphasic (E/I_2) patterns were changed to monophasic ones (E). In all cases, the PN response without the SK current consisted in a long tonic excitation (E phases in Fig. 2C), which disrupted the ability to track pheromone-like pulses (Fig. 2D). Given that the SK channel is sensitive to BIC, these results are in agreement with experimental data, showing that BIC prolongs PN excitation and compromises coding of intermittent pheromone pulses in *M. sexta* (30).

Efficient Coding of Pheromone: Dual Latency Coding Scheme. It is known that behavioral responses of male moths to pheromone signals are fast. However, the nature of the neural code that underlies rapid pheromone processing has been elusive. To examine candidate neural codes, we simulated the MGC model with inputs mimicking a mixture of BAL and C15 in different proportions and various concentrations. The binary mixture model was given by $K(P \times \text{BAL} + (1 - P) \times \text{C15})$, with K being the concentration and P being the proportion (*SI Text, Model*). In our model, $P = 2/3$ corresponds to the correct natural pheromone ratio (proportion of BAL two times as big as C15). Spike raster activities revealed three distinct populations of synchronized

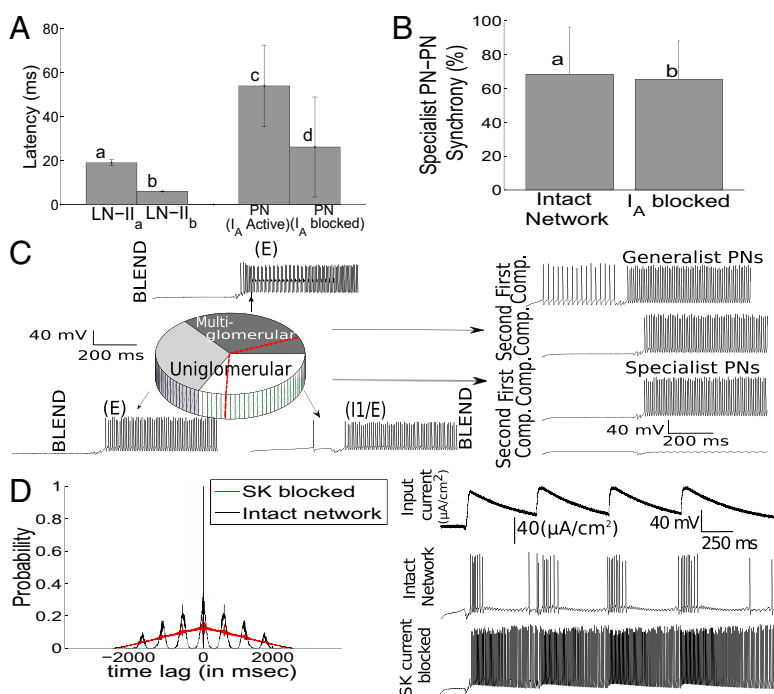


Fig. 2. Effects of removing I_A or I_{SK} . (A) First spike latencies were significantly shorter for LNs than PNs (19 ± 3 ms for LN-IIa and 3 ± 1.5 ms for LN-IIb vs. 54 ± 18 ms for PNs, $P < 0.05$, Kruskal–Wallis test followed by Mann–Whitney test). Without I_A , the PNs fired earlier (latency = 26 ± 22 ms, $P < 0.05$, Kruskal–Wallis test). (B) Without I_A , PNs were less synchronized. The percentage of synchronous spikes found in all pairs of specific PNs was $69 \pm 27\%$ for intact PNs vs. $66 \pm 23\%$ without I_A ($P < 0.05$, Kruskal–Wallis test). (C) Without I_{SK} , I_2 disappeared from the multiphasic responses. The original biphasic and triphasic patterns in B were changed, respectively, to monophasic (E) and biphasic (I1/E). The same proportions of 30%–37%–33% as in B were, thus, obtained for the generalists and monophasic and biphasic specialists, respectively. (D) Without I_{SK} , PNs lost pulse-tracking capability. The autocorrelation function was computed to quantify the capability of PNs to track pheromone-like pulses delivered at 1.67 Hz. For intact PNs, the autocorrelation function (black curve) presented periodic peaks separated by 600-ms intervals and corresponding to the stimulus interpulse interval. Without I_{SK} , the autocorrelation function was not periodic anymore (red curve). The alteration of the ability to track pheromone-like pulses is illustrated by comparing the response of a PN with or without I_{SK} (Right).

neurons: generalist PNs, specialist C15-PNs, and specialist BAL-PNs (Fig. S3A). Generalist PNs were the most activated neurons, because they received inputs from both glomeruli. As a consequence, they fired first, whereas specialist PNs fired later. With a mixture proportion of $P = 2/3$, the BAL-PNs were followed by the C15-PNs, because they received two times as much excitatory drive as the C15-PNs. The rank order of the three PN populations was consistent across repeated trials, despite random initial conditions thanks to the resetting of the PNs by I_1 (see above). In the context of fast processing, we asked whether first spike latency of the different PN populations could be used as a code. We, therefore, evaluated the information contained in a latency code compared with a rate code. The datasets for rate or latency contained three attributes (mean absolute latencies or mean firing rates of generalist, specialist C15, and specialist BAL populations), and the goal was to discriminate the correct proportion of $P = 2/3$ against incorrect mixture ratios (Methods). Both rate and latency datasets were almost linearly separable, which was revealed by plotting the average discriminant plane obtained by cross-validation (Fig. S3B and C). Classification performance was estimated by averaging the classification errors over the validation sets. It was higher with latency attributes than rate attributes, with an average 99.7% classification success with latency compared with 96.4% with rate (Fig. S3D). This result showed that a code based on latency would be efficient for rapid pheromone recognition, but it does not give any clue as to how concentration-invariant recognition could be achieved.

Interestingly, the normalized latency difference between C15 and BAL populations, computed as $(LBAL - LC15)/(LBAL + LC15)$, was found to be sensitive to the proportion P (red curve in Fig. 3B), behaving as $2P - 1$, but changed very little with

concentration (red curve in Fig. 3A). Despite relative concentration invariance, information on concentration was not lost. The mean absolute latency of the population of generalist PNs was found to be sensitive to changes in concentration K (black curve in Fig. 3A), while being invariant to changes in proportion (black curve in Fig. 3B). The MGC could, therefore, make use of latencies to implement a dual coding scheme, quantitative and qualitative (a theoretical explanation for this dual invariance coding scheme is provided in *SI Text* and Figs. S4–S6). However, latency coding makes sense only if one considers the first spike with respect to a reference signal [e.g., the first spike after stimulus onset (absolute latency as above) or after a particular event in the brain dynamics (relative latency)]. Because the stimulus onset is generally unknown to the brain, we looked at a putative internal reference signal from which to extract relative latencies. We found that the generalist PNs fired consistently with a delay of ~ 40 – 50 ms after stimulus onset. Compared with the specialist PNs, this delay was relatively constant across a wide range of proportions and concentrations (Figs. S5 and S6), suggesting that the firing of the generalist PN population could provide an internal reference for temporal marking. We, therefore, computed relative latencies of C15 and BAL PNs with respect to the generalist PN population. We found that the normalized difference in relative latencies encoded for the stimulus identity, being concentration-invariant (red curve in Fig. 3C) and proportion-sensitive (red curve in Fig. 3D), whereas the mean relative latency of specialist PNs encoded for the stimulus intensity, being concentration-sensitive (black curve in Fig. 3C) and proportion-invariant (black curve in Fig. 3D).

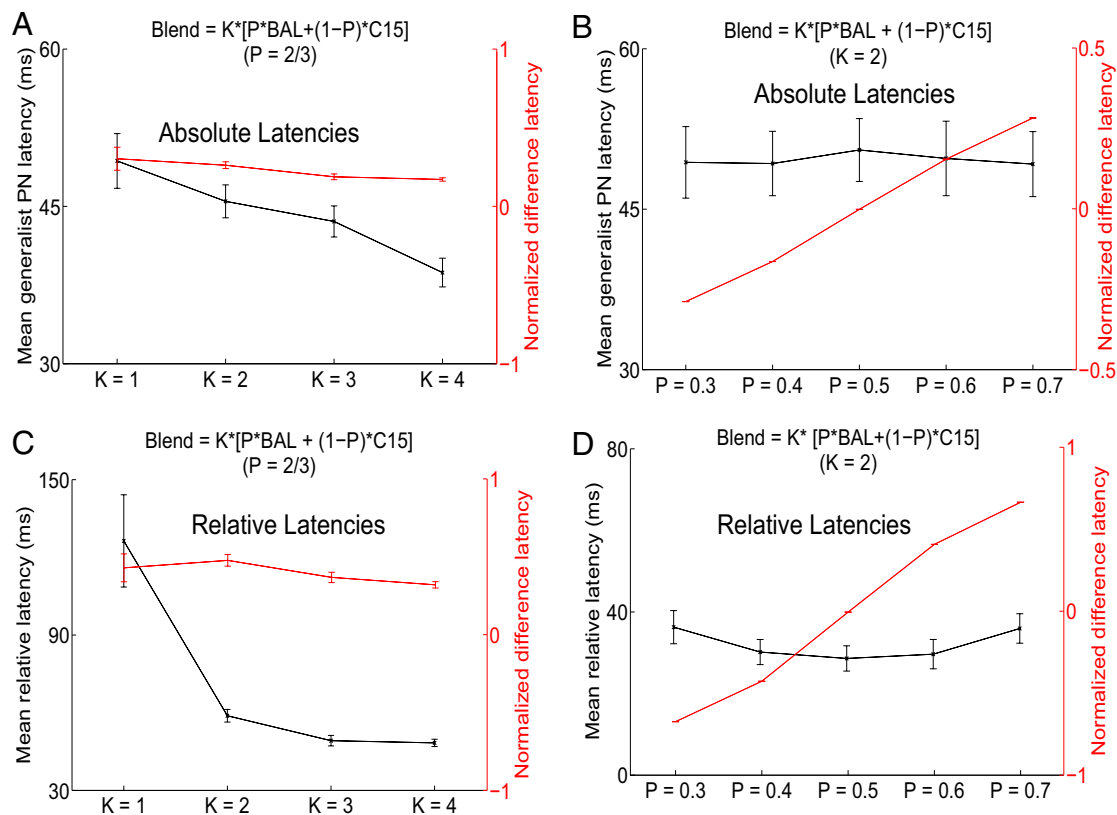


Fig. 3. Response latencies of the MGC model to blend-like stimuli in different proportions P and concentrations K . The binary mixture model is $K(P \times BAL + (1 - P) \times C15)$. (A) Dependence of concentration K on latency. On the one hand, the latency of the generalist PNs multiglomerulus was sensitive to changes in concentration K (black curve). On the other hand, the normalized latency difference $(LC15 - LBAL)/(LBAL + LC15)$ between C15 and BAL PNs changed very little with concentration (red curve). (B) Dependence of proportion P on latency. The normalized latency difference behaved as $2P - 1$ (red curve), whereas the latency of the generalist PNs was invariant to changes in proportion (black curve). (C and D) Same as in A and B but for the relative latencies of C15 and BAL PNs computed with respect to the generalist PN population.

Discussion

When flying in a turbulent plume, male moths encounter intermittent pheromone patches. Their short duration puts a strong temporal pressure on the olfactory system (13, 14). In the context of fast pheromone processing, we suggested that latency to the first spike could be used as information carrier. Evidence for latency coding has been found in diverse neuronal structures such as the visual system (31–33), the tactile system (34), and the olfactory system (35–37). Latency coding often implies sensing the external world as a discrete sequence of events. In the visual system, sudden movements of the eyes, called saccades, sample the visual input into discrete snapshots. After each saccade, a new image is encoded into first spike latencies to be further processed by the brain. Similarly to the saccades in vision, sniffing in rodents samples the olfactory scene into discrete odor puffs. In each of these cases, the stimulus onset is actively controlled by the brain. In the case of moths, however, the pheromone plume is broken up into discrete filaments by the turbulent medium and not by an internal sampling mechanism. Under this condition, what could be the internal reference signal from which to extract latencies? Our MGC model suggests that generalist PNs serve as a temporal marker to compute relative latencies of specialist PNs. Interestingly, normalized latency differences of specialist PNs carried concentration-invariant information about pheromone blend identity. Subtraction and normalization to achieve invariance were previously reported. In the salamander visual system, differences in response latency of retina cells were found to be invariant to stimulus contrast (33). In the rat olfactory bulb, normalization of glomerular responses has been proposed as a means to achieve invariance in concentration (38), and we have suggested a mechanism of competition by lateral inhibition in the moth MGC in a separate model (39). From this coding perspective, the novelty of the work presented here lies in the use of response latencies for signaling the correct component ratio rather than the presence of network oscillations (40) or specific rate patterns (41). A latency code allows much faster responses and therefore, seems best suited to address the tight time constraints of pheromone blend detection in a turbulent plume. Another important point in our model is that, despite relative concentration invariance, information on concentration was not lost as the mean latency of specialist PNs encoded for stimulus intensity. The MGC of *M. sexta* moths could, therefore, make use of latencies to implement a dual coding scheme and resolve the apparent contradiction between quantitative coding (sensitive to changes in concentration and invariant to changes in proportion) and qualitative coding (sensitive to changes in proportion and invariant to changes in concentration). As an extension to this work, the proposed latency coding scheme provided a direct input for designing bio-inspired data analysis methods for artificial olfaction in electronic noses (42).

In latency coding, one considers the neurons as analog to delay converters: the most strongly activated neurons tend to fire first, whereas more weakly activated cells fire later or not at all. Random initial conditions may, however, jeopardize this ideal situation by introducing variability in the time to first spike. The simulations presented in this article showed that this condition is not the case. Inhibition I_1 from LNs before the PN responses played the role of a reset by transiently driving the PNs to a common hyperpolarized state. As a consequence, PN latencies after stimulus onset depended more on the strength of the input than initial conditions. Generalist PNs fired first followed by BAL and C15 PNs (Fig. S3A). The rank order of the three groups reflected the intensity of their inputs. Within each group, PN synchrony arose as a consequence of inhibitory reset and shared ORN excitation. This type of synchronization is non-oscillatory and was observed experimentally in the MGC of *M. sexta* moths (21, 43). It differs from the 30- to 40-Hz oscillatory synchronization found in the generalist olfactory system of the same moth species (44). With nonpheromonal odors, the LNs are mainly driven by the PNs, and therefore, PN-LN interplay generates rhythmic inhibition and creates field potential oscillations (45–48). In contrast, our MGC model is essentially feed-

forward, lacking excitatory connections from PNs to LNs. The LNs are, thus, driven by ORN inputs and adapt rapidly. Consequently, the PNs are reset by a single strong inhibitory phase I_1 and fire synchronously when I_1 ends. This type of nonoscillatory synchronization persisted with added excitatory connections from PNs to LNs, provided that they are weak enough (strong PN-LN excitatory connections elicited fast ~40-Hz oscillations in our model) (SI Text and Fig. S7).

A prerequisite for the inhibitory reset I_1 is that LNs fire before PNs. In our MGC model, spike latencies were significantly shorter for LNs than PNs. PN firing was delayed by about 50 ms with respect to the fastest LNs, and this delay was attributable to the A current in PNs (Fig. 2A). In line with our results, time lags of about 60 ms have been reported between LN and PN firing latencies in the bee antennal lobe (49). Transient A-type K^+ currents have been identified in the PNs of *M. sexta* moths (27, 28). However, characterizing their potential involvement in modulating the time to first spike needs additional experimental studies.

The various response patterns observed experimentally in *M. sexta* projection neurons were reproduced in our MGC model by a combination of intrinsic K^+ currents (A-type or Ca^{2+} -dependent K^+) and network mechanisms (inhibition from LNs) rather than by varying the connectivity as in ref. 50. These intrinsic currents allowed the PNs to encode fast pulses of pheromone, despite long-lasting ORN responses. The ability to track intermittent stimuli was largely because of an intrinsic Ca^{2+} -dependent K^+ channel that produced I_2 and thereby, prevented PN responses of excessive duration. Ca^{2+} -dependent K^+ currents have been found in the PNs of *M. sexta* moths, but their type was not identified (28). A Ca^{2+} -dependent K^+ current has been incorporated in another modeling study as a mechanism of spike frequency adaptation to reproduce the slow patterning observed in the generalist system (51). For *M. sexta* moths, our model suggests that the Ca^{2+} -dependent K^+ current involved in I_2 could be of the SK type. This prediction is supported by experimental data revealing that I_2 is abolished by BIC and not PTX (22), a difference explained by the fact that the SK channel is BIC-sensitive (25, 26). To our knowledge, SK channels in insects have been shown only in a visual interneuron of the locust (52). A direct confirmation of the existence of SK channels in *M. sexta* moths is, therefore, needed. However, this task is not easy to accomplish, because the most common antagonist, apamin, has no effect in insects (52).

Methods

Network Simulations. The simulated MGC model consisted of 86 LNs-IIa, 68 LNs-IIb, and 41 PNs, and these numbers were grounded experimentally (18, 29). LNs and PNs were modeled as one compartment conductance-based models involving ionic currents and leak (SI Text, Model). In *M. sexta*, the LNs are multiglomerular, but most of the PNs are uniglomerular (53). We, therefore, modeled the LNs as multiglomerular. Uni- and multiglomerular PNs were randomly chosen with probabilities of 0.7 and 0.3, respectively. Uniglomerular PNs were connected with equal probability to either one or the other glomerulus (toroid-BAL or cumulus-C15). The glomerular input model is detailed in SI Text, Model. Inhibitory LNs, IIa and IIb, were randomly connected to the PNs with probabilities of $p(\text{LN-IIa} \rightarrow \text{PN})$ and $p(\text{LN-IIb} \rightarrow \text{PN})$. The effect of these probabilities on the firing response patterns was studied above (Results). Physiological firing patterns were best reproduced with the intact MGC network and $p(\text{LN-IIa} \rightarrow \text{PN}) = 0.5$ and $p(\text{LN-IIb} \rightarrow \text{PN}) = 0.2$. These probabilities were also used in the simulations with noninsect networks. The GABA_A synaptic model from LNs to PNs was adapted from ref. 54 and is detailed in SI Text, Model. Network simulations were performed with SIRENE, a C-based neural simulator developed by our team and available at <http://sirene.gforge.inria.fr>. The ordinary differential equations are numerically integrated with a classical fourth-order Runge-Kutta method with a time step of 0.01 ms.

Data Analyses. We identified the PNs' types from the response to single compounds. PNs were considered as specialist or generalist according to whether they were excited by one compound only or by the two compounds presented individually. Excitation E was detected if at least one spike was found within 100 ms after stimulus onset. Inhibition I_1 was detected whenever a hyperpolarization of the membrane potential occurred right

after stimulus onset. To determine hyperpolarization, the membrane potential was filtered (fourth-order low-pass Butterworth, 50-Hz cutting frequency) and averaged before and after stimulus onset (averaging window of 200 ms before and 80 ms after stimulus onset). Inhibition I_2 was determined from visual inspection. To quantify the plausibility of the model, the proportion of response patterns (combination of I_1 , E , and I_2) was compared with the real proportion observed in experimental data by computing the KLD (*SI Text, Model*). Synchrony between two PNs was quantified as the percentage of synchronous spikes (maximum time lag ± 2.5 ms) relative to the total number of spikes as in ref. 21. The synchrony level was expressed as the mean synchrony computed for all pairs of uniglomerular PNs. Classification performance was estimated for the two coding schemes: rate and latency. Absolute latency and mean firing rate were computed as, respectively, the time to first spike and the number of spikes within a 200-ms window after stimulus onset. The classification task was to discriminate the correct proportion of $P = 2/3$ at concentrations K (80 samples for $P = 2/3$ and $K = 1, 2, 3, 4$) against incorrect mixture ratios (100 samples for $P = 0.3, 0.4, 0.5,$

$0.6, 0.7$ and $K = 1$). The dataset for rate or latency contained 180 samples of three inputs (mean absolute latencies or mean firing rates of generalist, specialist C15, and specialist BAL populations). The training set consisted of 90 samples taken randomly from the entire dataset, and the test set consisted of the remaining 90 samples. Training and test sets were resampled 10 times to estimate the cross-validation error. A linear support vector machine (SVM) with parameter one was used as classifier (55). All data analyses and statistical tests were performed in Matlab (www.mathworks.com) except for the classification performance, which was assessed with a custom-made SVM program.

ACKNOWLEDGMENTS. We are grateful to Dr. Philippe Lucas for helpful discussions. This work was funded by the French and British national agencies [Agence Nationale de la Recherche (ANR), Biotechnology and Biological Sciences Research Council (BBSRC)] in a coordinated manner for Collaborative Research in Systems Biology Grant BSYS-006-02-PHEROSYS and European Research Project "Biologically inspired computation for chemical sensing" Grant FP7-216916-NEUROCHEM.

- Pope MM, Gaston LK, Baker TC (1982) Composition, quantification and periodicity of sex pheromone gland volatiles from individual *Heliothis virescens* females. *J Chem Ecol* 8:1043–1055.
- Pope MM, Gaston LK, Baker TC (1984) Composition, quantification, and periodicity of sex pheromone volatiles from individual *Heliothis zea* females. *J Insect Physiol* 30:943–945.
- Löfstedt C, Herrebout WM, Menken SBJ (1991) Sex pheromones and their potential role in the evolution of reproductive isolation in small ermine moths (Yponomeutidae). *Chemoecology* 2:20–28.
- Glover TJ, Tang X-H, Roelofs WL (1987) Sex pheromone blend discrimination by male moths from E and Z strains of European corn borer. *J Chem Ecol* 13:143–151.
- Linn CE, Young MS, Gendle M, Glover TJ, Roelofs WL (1997) Sex pheromone blend discrimination in two races and hybrids of the European corn borer moth, *Ostrinia nubilalis*. *Physiol Entomol* 22:212–223.
- Willis MA, Baker TC (1988) Effects of varying sex pheromone component ratios on the zigzagging flight movements of the oriental fruit moth, *Grapholitha molesta*. *J Insect Behav* 1:357–371.
- Liu Y-B, Haynes KF (1992) Filamentous nature of pheromone plumes protects integrity of signal from background chemical noise in cabbage looper moth, *Trichoplusia ni*. *J Chem Ecol* 18:299–307.
- Jones C (1983) On the structure of instantaneous plumes in the atmosphere. *J Hazard Mater* 7:87–112.
- Riffell JA, Abrell L, Hildebrand JG (2008) Physical processes and real-time chemical measurement of the insect olfactory environment. *J Chem Ecol* 34:837–853.
- Laurent G, Davidowitz H (1994) Encoding of olfactory information with oscillating neural assemblies. *Science* 265:1872–1875.
- Laurent G, Wehr M, Davidowitz H (1996) Temporal representations of odors in an olfactory network. *J Neurosci* 16:3837–3847.
- Laurent G (1999) A systems perspective on early olfactory coding. *Science* 286:723–728.
- Vickers NJ, Christensen TA, Baker TC, Hildebrand JG (2001) Odour-plume dynamics influence the brain's olfactory code. *Nature* 410:466–470.
- Baker TC, Hansson BS, Löfstedt C, Löfqvist J (1988) Adaptation of antennal neurons in moths is associated with cessation of pheromone-mediated upwind flight. *Proc Natl Acad Sci USA* 85:9826–9830.
- Bhandawat V, Maimon G, Dickinson MH, Wilson RI (2010) Olfactory modulation of flight in *Drosophila* is sensitive, selective and rapid. *J Exp Biol* 213:3625–3635.
- Tumlinson JH, et al. (1989) Identification of a pheromone blend attractive to *Manduca sexta* (L.) males in a wind tunnel. *Arch Insect Biochem Physiol* 10:255–271.
- Kaissling KE, Hildebrand JG, Tumlinson JH (1989) Pheromone receptor cells in the male moth *Manduca sexta*. *Arch Insect Biochem Physiol* 10:273–279.
- Christensen TA, Hildebrand JG (1987) Male-specific, sex pheromone-selective projection neurons in the antennal lobes of the moth *Manduca sexta*. *J Comp Physiol A Neuroethol Sens Neural Behav Physiol* 160:553–569.
- Kanzaki R, Soo K, Seki Y, Wada S (2003) Projections to higher olfactory centers from subdivisions of the antennal lobe macroglomerular complex of the male silkworm. *Chem Senses* 28:113–130.
- Haupt SS, Sakurai T, Namiki S, Kawata T, Kanzaki R (2010) Olfactory information processing in moths. *The Neurobiology of Olfaction*, ed Menini A (CRC, Boca Raton, FL), pp 71–112.
- Lei H, Christensen TA, Hildebrand JG (2002) Local inhibition modulates odor-evoked synchronization of glomerulus-specific output neurons. *Nat Neurosci* 5:557–565.
- Waldrop B, Christensen TA, Hildebrand JG (1987) GABA-mediated synaptic inhibition of projection neurons in the antennal lobes of the sphinx moth, *Manduca sexta*. *J Comp Physiol A Neuroethol Sens Neural Behav Physiol* 161:23–32.
- Zhang HG, Lee HJ, Rocheleau T, French-Constant RH, Jackson MB (1995) Subunit composition determines picrotoxin and bicuculline sensitivity of *Drosophila* gamma-aminobutyric acid receptors. *Mol Pharmacol* 48:835–840.
- Christensen TA, Waldrop BR, Hildebrand JG (1998) Multitasking in the olfactory system: Context-dependent responses to odors reveal dual GABA-regulated coding mechanisms in single olfactory projection neurons. *J Neurosci* 18:5999–6008.
- Khawaled R, Bruening-Wright A, Adelman JP, Maylie J (1999) Bicuculline block of small-conductance calcium-activated potassium channels. *Pflügers Arch* 438:314–321.
- Debarbieux F, Brunton J, Charpak S (1998) Effect of bicuculline on thalamic activity: A direct blockade of I_{AHP} in reticularis neurons. *J Neurophysiol* 79:2911–2918.
- Mercer AR, Hayashi JH, Hildebrand JG (1995) Modulatory effects of 5-hydroxytryptamine on voltage-activated currents in cultured antennal lobe neurons of the sphinx moth *Manduca sexta*. *J Exp Biol* 198:613–627.
- Mercer AR, Hildebrand JG (2002) Developmental changes in the density of ionic currents in antennal-lobe neurons of the sphinx moth, *Manduca sexta*. *J Neurophysiol* 87:2664–2675.
- Matsumoto SG, Hildebrand JG (1981) Olfactory mechanisms in the moth *Manduca sexta*: Response characteristics and morphology of central neurons in the antennal lobes. *Proc R Soc Lond B Biol Sci* 213:249–277.
- Lei H, Riffell JA, Gage SL, Hildebrand JG (2009) Contrast enhancement of stimulus intermittency in a primary olfactory network and its behavioral significance. *J Biol* 8:21.
- Van Rullen R, Thorpe SJ (2001) Rate coding versus temporal order coding: What the retinal ganglion cells tell the visual cortex. *Neural Comput* 13:1255–1283.
- Gawne TJ, Kjaer TW, Richmond BJ (1996) Latency: Another potential code for feature binding in striate cortex. *J Neurophysiol* 76:1356–1360.
- Gollisch T, Meister M (2008) Rapid neural coding in the retina with relative spike latencies. *Science* 319:1108–1111.
- Johansson RS, Birnieks I (2004) First spikes in ensembles of human tactile afferents code complex spatial fingertip events. *Nat Neurosci* 7:170–177.
- Hopfield JJ (1995) Pattern recognition computation using action potential timing for stimulus representation. *Nature* 376:33–36.
- Margrie TW, Schaefer AT (2003) Theta oscillation coupled spike latencies yield computational vigour in a mammalian sensory system. *J Physiol* 546:363–374.
- Junek S, Kludt E, Wolf F, Schild D (2010) Olfactory coding with patterns of response latencies. *Neuron* 67:872–884.
- Clelland TA, Johnson BA, Leon M, Linster C (2007) Relational representation in the olfactory system. *Proc Natl Acad Sci USA* 104:1953–1958.
- Zavada A, Buckley CL, Martinez D, Rospars J-P, Nowotny T (2011) Competition-based model of pheromone component ratio detection in the moth. *PLoS One* 6:e16308.
- Linster C, Kerszberg M, Masson C (1994) How neurons may compute: The case of insect sexual pheromone discrimination. *J Comput Neurosci* 1:231–238.
- Kwok YC (2007) Encoding of odour blends in the moth antennal lobe. PhD thesis (University of Leicester, Leicester, UK).
- Chen HT, Ng KT, Bernak A, Law MK, Martinez D (2011) Spike latency coding in a biologically inspired microelectronic nose. *IEEE Trans Biomed Circuits Syst* 5:160–168.
- Christensen TA, Lei H, Hildebrand JG (2003) Coordination of central odor representations through transient, non-oscillatory synchronization of glomerular output neurons. *Proc Natl Acad Sci USA* 100:11076–11081.
- Ito I, Bazhenov M, Ong RC, Raman B, Stopfer M (2009) Frequency transitions in odor-evoked neural oscillations. *Neuron* 64:692–706.
- Börgers C, Kopell N (2003) Synchronization in networks of excitatory and inhibitory neurons with sparse, random connectivity. *Neural Comput* 15:509–538.
- Kopell N, Ermentrout B (2004) Chemical and electrical synapses perform complementary roles in the synchronization of interneuronal networks. *Proc Natl Acad Sci USA* 101:15482–15487.
- Martinez D (2005) Oscillatory synchronization requires precise and balanced feedback inhibition in a model of the insect antennal lobe. *Neural Comput* 17:2548–2570.
- Martinez D, Montejó N (2008) A model of stimulus-specific neural assemblies in the insect antennal lobe. *PLoS Comput Biol* 4:e1000139.
- Krofczik S, Menzel R, Nawrot MP (2009) Rapid odor processing in the honeybee antennal lobe network. *Front Comput Neurosci* 2:9.
- Linster C, Masson C, Kerszberg M, Personnaz L, Dreyfus G (1993) Computational diversity in a formal model of the insect olfactory macroglomerulus. *Neural Comput* 5:228–241.
- Sivan E, Kopell N (2006) Oscillations and slow patterning in the antennal lobe. *J Comput Neurosci* 20:85–96.
- Peron S, Gabbiani F (2009) Spike frequency adaptation mediates looming stimulus selectivity in a collision-detecting neuron. *Nat Neurosci* 12:318–326.
- Homborg U, Christensen TA, Hildebrand JG (1989) Structure and function of the deutocerebrum in insects. *Annu Rev Entomol* 34:477–501.
- Skinner FK, Chung JY, Ncube I, Murray PA, Campbell SA (2005) Using heterogeneity to predict inhibitory network model characteristics. *J Neurophysiol* 93:1898–1907.
- Burges CJ (1998) A tutorial on support vector machines for pattern recognition. *Data Mining and Knowledge Discovery* 2:121–167.